



Uniaxial Compression Creep Characteristics and Acoustic Emission Characteristics of Two Different Kinds of Red Sandstone with Different Particle Sizes

Kui Zhao¹ · Liangxiao Xiong^{2,3} · Zeliang Kuang¹ · Zhongyuan Xu⁴ · Peng Zeng¹

Received: 2 February 2021 / Accepted: 5 May 2021 / Published online: 25 May 2021
© King Fahd University of Petroleum & Minerals 2021

Abstract

In this study, we tested uniaxial compression deformation and uniaxial compression creep on red sandstone specimens with fine- and medium-sized particles; microstructure development and acoustic emission (AE) were recorded. The creep deformation characteristics and AE parameters of these two kinds of sandstone specimens were then compared and analysed. Results show that the microstructure of fine-grained sandstone is the granular sand-like structure, and the medium-grained sandstone has a grain-like microstructure. The particle size obviously influences uniaxial compressive mechanism; the medium-grained sandstone has a higher creep deformation than the fine-grained sandstone, while the AE amplitude, AE event rate and AE ring-down count rate of the medium- and fine-grained sandstone specimens have similar trend during the creep stage. The failure of both medium- and fine-grained sandstone mainly occurs in the transient and accelerated creep stages during the creep process. By combining the variation of AE parameters and AE-*r* value (the ratio of the accumulative hits and the cumulative energy) in the various creep stages, we found the creep damage to sandstone could be predicted to a certain extent.

Keywords Red sandstone · Uniaxial compression creep test · Acoustic emission

✉ Liangxiao Xiong
xionglx1982@126.com

Kui Zhao
296931654@qq.com

Zeliang Kuang
403997188@qq.com

Zhongyuan Xu
zyxu@udel.edu

Peng Zeng
402230385@qq.com

¹ School of Resources and Environment Engineering, Jiangxi University of Science and Technology, Ganzhou 341000, Jiangxi Province, China

² School of Civil Engineering and Architecture, East China Jiaotong University, Nanchang 330013, China

³ Guangxi Key Laboratory of Disaster Prevention and Engineering Safety, Guangxi University, Nanning 530004, China

⁴ Department of Earth Sciences, University of Delaware, Newark, DE 19716, USA

1 Introduction

The creep property is one of the inherent characteristics of rock and is closely related to long-term stability and safety in rock engineering. To date, many scholars have conducted a large number of indoor compression creep tests. There are many factors affecting the creep properties of rock, including microstructure and particles. A few researchers have studied the influence of microstructure and particle size on the creep properties of rock. Xiong et al. [1] conducted biaxial compression creep tests on greenschist and found that the volumetric content of the marble interlayer has an obvious effect on creep deformation. Chen [2] carried out creep tests on silty mudstone with two different particle sizes, they indicated that the strength of silty mudstone decreases, while steady creep rate increases with the increase in grain size. However, the influence of microstructure and particle size on rock creep characteristics is still unclear which needs to be further investigated.

Acoustic emission (AE) is a phenomenon associated with the internal structure evolution of rock. It is a good indicator to describe the changing state of the internal microstructure and therefore reflects the evolution process of rock damage.



The investigation and analysis of rock creep process through acoustic emission has become an effective method to monitor creep damage and destruction. Ohnaka [3] found that the AE activity of brittle rock under a constant load to failure is divided into primary, secondary and tertiary phases. Yang et al. [4] showed that AE activities of coal specimens gradually increase with the expansion of the micro-pores and micro-fractures during the transient creep stage; the AE events decrease during the steady creep stage and reach the maximum value during the accelerated creep stage. Gong et al. [5] studied the AE of the red sandstone during short-time creep. They found that the AE event rates and energy rates decrease with time during the period from decelerated creep to steady creep, and the AE amplitude transition frequency increases obviously during the accelerated creep stage. Chen et al. [6] indicated that stress cycling transiently increases with the strain rate and the AE activity rate during unloading and loading creep tests. Li et al. [7] found that the ring-down count rate and creep rate of sandstone have a same trend. Shi et al. [8] carried out AE experiments to study short-time creep behaviour under uniaxial compression for cuboid-shaped fine sandstone specimens with two pre-existing cracks; the results showed that the AE events well reflect the crack evolution process of specimens with cracks. Zhu et al. [9] found that under the same creep stress, a dynamic disturbance with higher impact energy results in a higher axial strain rate, absolute volumetric strain rate and AE energy rate. Zeng et al. [10] found that the AE parameters are consistent with the creep strain of salt rock. Yang et al. [4], Li et al. [7] and Zhu et al. [9] reached a consensus that AE ring-down count rate is high in the decelerating creep phase and low in the even creep phase, it may sudden increase evolved from even to accelerating creep phase.

The stress level in conducting a rock creep test was referring to the crack initiation stress (σ_{ci}) and critical damage stress (σ_{cd}). When the applied stress level is between σ_{ci} and σ_{cd} , the cracks inside the rock accumulate and grow in a steady rate. If the axial stress is maintained at a stress level above σ_{cd} , accelerated creep rates may occur which leads to a sudden failure of the specimen [11].

Many researchers have determined σ_{ci} , σ_{cd} and σ_{ucs} (uniaxial compressive strength) of different rocks through experiments. Nicksiar et al. [12] found that for igneous, sedimentary and metamorphic rocks, the ratio of σ_{ci}/σ_{ucs} ranges from 0.42 to 0.47 regardless of the material properties in uniaxial compression, whereas this ratio ranges from 0.50 to 0.54 when it is confined. Xue et al. [13] pointed out that overall averages of σ_{cd}/σ_{ucs} for igneous, metamorphic, and sedimentary rocks are about 0.78, 0.85 and 0.73, respectively. Kim et al. [14] found that the ratio of σ_{ci}/σ_{ucs} is about 0.42–0.53 and the ratio of σ_{cd}/σ_{ucs} is about 0.62–0.84 for granite. Pepe et al. [15] showed that the ratios of σ_{ci}/σ_{ucs} are about 0.46 and 0.49 for

metamorphic and sedimentary rocks, respectively, and the ratios of σ_{ci}/σ_{ucs} are about 0.85 and 0.90 for metamorphic and sedimentary rocks, respectively. Li et al. [16] found that the ratios of σ_{ci}/σ_{ucs} for igneous, metamorphic and sedimentary rocks are 0.79, 0.81 and 0.82, respectively. Zhang et al. [17] pointed out that the ratio of σ_{ci}/σ_{ucs} of granite samples estimated by strain-based method ranges from 0.4 to 0.55, and 0.49–0.6 by wave transmission method, both are higher than that of acoustic emission method (0.38–0.46).

The experimental study on creep characteristics and acoustic emission characteristics of rock is still seldom, and these researchers only focused on one or two indicators of AE test. For example, Yang et al. [4] mainly analysed the ring-down count rate, Li et al. [7] mainly examined AE ring-down count and cumulative AE ring-down count, and Zhu et al. [9] investigated AE cumulative energy and cumulative AE count rate. The research on the compound effect of AE amplitude, AE event rate and AE- r value is still seldom. Otherwise, the microstructure of rock also contributes a lot to the creep and AE characteristics, while the related research achievements are still missing. This study took red sandstone as its research object including sandstone with fine-sized particles and sandstone with medium-sized particles. Uniaxial compression creep tests under a constant load and AE tests were used, the creep deformation characteristics, AE amplitude, AE event rate and AE ring-down count rate and AE- r value were compared and analysed.

2 Test Equipment, Specimen Characteristics and Test Groups

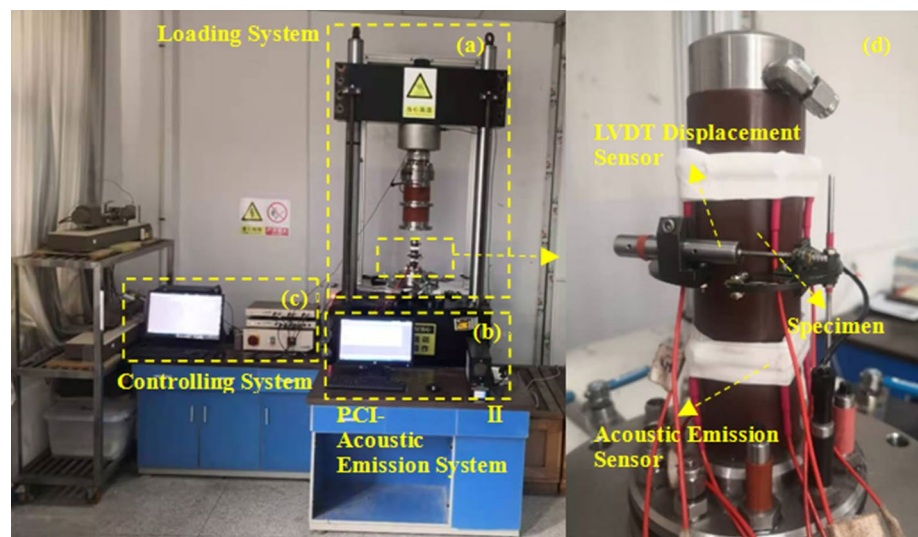
2.1 Test Equipment

The uniaxial compression creep test was performed by using a GDS-HPTAS triaxial rheological testing machine (GDS Instruments), as shown in Fig. 1. This machine has a maximum axial load of 400 kN and a range of 0–32 MPa of confining pressure.

In the compression creep test, the axial strain of the specimen is obtained by using the LVDT (Linear Variable Differential Transformer) of GDS. In the uniaxial compression test, the axial and lateral strains of the sample are measured by LVDT and strain gauges.

The AE system contains an AE acquisition board (PCI-2; Physical Acoustics, USA) and control software (AE-win; Physical Acoustics). The system has 8 channels, and one AE sensor was placed on the cylindrical surface which is in the middle of specimen (Fig. 1). The AE parameters in this study are directly obtained from this system without post-processing.

Fig. 1 GDS-HPTAS triaxial rheological testing machine and AE system



2.2 Specimen Characteristics

The sandstone specimens used in the experiment were taken from an open quarry in the southwestern part of Jiangxi Province in China. Two sandstone blocks were collected from this site, labelled as ‘M’ and ‘L’.

Core samples were taken from blocks, and cut by an automatic rock cutting machine. Then the rock sample was polished into a cylindrical standard specimen, diameter is 50 mm, and height is 100 mm. Cylindrical specimens drilled from blocks M and L were defined as Class M and Class L sandstone, respectively. The microstructures of Class M and L sandstone under 4X microscope are shown in Fig. 2. After processing, the rock specimens were dried in an oven at 110 °C for 2 days.

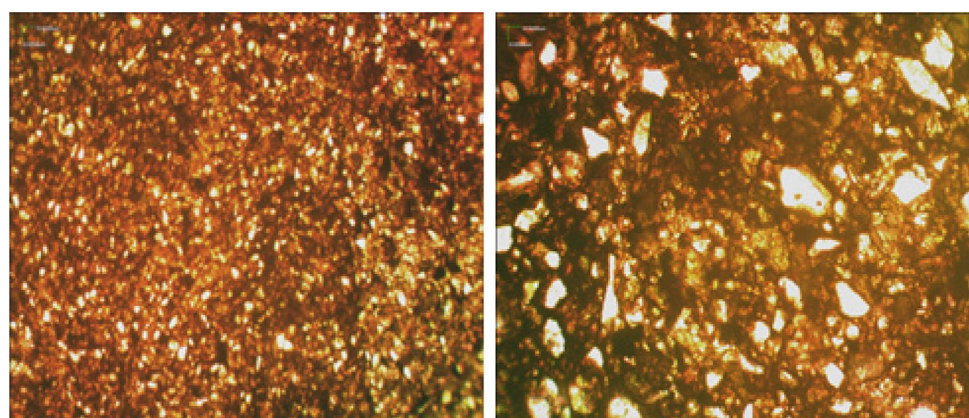
The microstructure of Class M sandstone is the granular sand-like structure, with 90% sand particle and 10% filler. The diameter of sand particles ranges from 0.05 to

0.1 mm, and their sorting property is good. The major content of the sand particles is quartz with some feldspar and a small amount of muscovite. The filler is mainly calcium and iron cement.

The Class L sandstone has a grain-like microstructure with 91% sand and 9% filler. Most of the sand particles have diameters ranging from 0.1 to 0.5 mm, a small portion ranges from 1.0 to 1.5 mm, and some individual sand particles have diameters ranging from 1.5 to 2.0 mm. Quartz accounts for 85% and feldspar accounts for 15% of their content. The clastic filler material is dominated by muscovite and heavy minerals, and the cement is the same as that in Class M sandstone.

Therefore, according to the size of the constituent particles, Class L sandstone is referred to as medium-grained sandstone, whereas Class M sandstone is referred to as fine-grained sandstone. In general, there are a total of 18 fine-grained sandstone specimens and 24 medium-grained sandstone specimens.

Fig. 2 Microstructures of classes M and L sandstone under 4X microscope



(a) Class M sandstone

(b) Class L sandstone

2.3 Experimental Groups

The experimental study was performed at room temperature (20 ± 2 °C). The specimens were allocated as described below.

2.3.1 Uniaxial Compression Test

Uniaxial compression deformation tests were carried out using four Class L sandstone specimens and four Class M sandstone specimens. The four Class L sandstone specimens were labelled as L1#, L2#, L3# and L4#, and the four Class M specimens were labelled as M1#, M2#, M3# and M4#.

2.3.2 Uniaxial Compression Creep Test and Acoustic Emission Test

The uniaxial compression creep and AE tests were carried out using three Class L sandstone specimens and three Class M sandstone specimens. The three Class L sandstone specimens were labelled as L5#, L7# and L24#, and the three Class M specimens were labelled as M5#, M6# and M16#.

3 Uniaxial Compression Test Results of these Two Kinds of Sandstone

The relationship curves of the stress, total volumetric strain and crack volumetric strain of specimens L1# and M1# are shown in Fig. 3.

In Fig. 3, ϵ_1 is the axial strain, ϵ_v^c is the crack volumetric strain, ϵ_v is the total volumetric strain, σ_1 is the axial stress, σ_{ci} is the crack initiation stress and σ_{cd} is the crack damage stress.

The calculation of ϵ_v is as follows:

$$\epsilon_v = \epsilon_1 + 2\epsilon_3 \tag{1}$$

where ϵ_1 is the axial strain, and ϵ_3 is the lateral strain.

Martin et al. (1993) defined the crack volumetric strain (ϵ_v^c) as the elastic volumetric strain (ϵ_v^e) subtract from total volumetric strain (ϵ_v), the expression is

$$\epsilon_v^c = \epsilon_v - \epsilon_v^e = \epsilon_v - \frac{1 - 2\mu}{E} \sigma_1 \tag{2}$$

where ϵ_v^e is the elastic volumetric strain, μ is Poisson’s ratio and E is Young’s modulus.

E and μ are constant [14, 18], and can be calculated from the stress–strain curve when the deviatoric stress is one-half of the compressive strength [19].

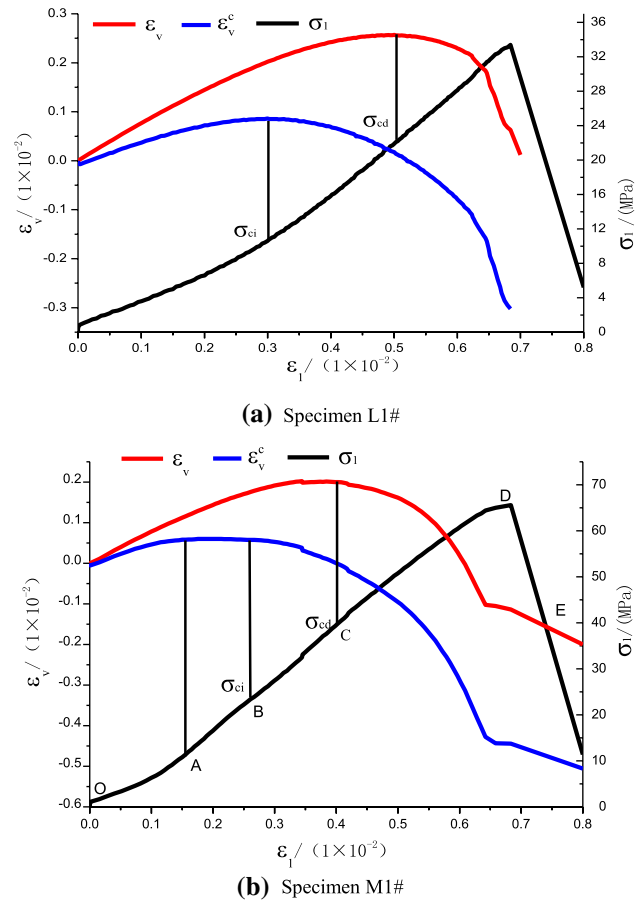


Fig. 3 Relationship curves of stress, total volumetric strain and crack volumetric strain of specimens L1# and M1#

σ_{ci} is defined as the onset of stable crack growth and indicates the point at which the crack volumetric strain deviates from zero, that is the endpoint of the horizontal line segment of crack volumetric strain curve [14, 20]. σ_{cd} is characterized by unstable crack growth; it is determined by the inflection point of total volumetric strain curve [14, 20].

Taking specimen M1# in Fig. 3 as an example, the stress–strain curves among the stress, total volumetric strain and crack volumetric strain can be divided into the following four stages:

3.1 OA Stage (Initial Crack Closure Stage)

During the initial crack closure stage of sandstone, the stress–strain curve generally shows an “upward concave” shape, which indicates the compacting of original crack or void. At this time, the crack volumetric strain rises, whereas the growth rate slows down with time. The total volumetric strain is also in a state of constant growth.

3.2 AB Stage (Elastic Compression Stage)

In this stage, the axial stress shows a linear relationship with strain, and new microcracks rarely occur during this stage. The upper limit of this stage is the crack initiation stress, which is the trigger for the initiation and development of cracks, it is also the initial stress of the rock begin to expand. The crack initiation stress of sandstone specimen is about one fourth of the uniaxial compressive strength.

3.3 BC Stage (Stable Growth Stage of Crack)

When the external load exceeds the crack initiation strength of the rock, new microcracks begin to generate inside the rock. At this time, the crack volumetric strain curve begins to develop in reverse, from crack closure to the crack propagation state. The growth rate of the total volumetric strain decreases with time. The stress corresponding to the end of this stage is σ_{cd} , which was about 1/2–3/4 of the uniaxial compressive strength of sandstone.

3.4 CD Stage (Crack Accelerating Growth Stage)

In this stage, the external load continues to increase. When the stress applied to the specimen is greater than σ_{cd} , the microcracks formed inside the rock connect and cause irreversible deformation. The total volumetric strain of the rock specimen changes from the previous volume compression to the volume expansion state, i.e. the total volume of the specimen alters from decline to increase. The crack growth rate is increasing, which eventually leads to the instability of the rock specimen. This phenomenon, in which the volume begins to increase, is called expansion. As the external load continues increasing, the stress on the specimen reaches the uniaxial compressive strength, the specimen undergoes

instability and damage, resulting in macroscopic surface fracture, and the specimen loses its load-bearing capacity.

The uniaxial compression mechanics parameters of medium- and fine-grained sandstone specimens are shown in Tables 1 and 2, respectively.

The mechanical parameters such as uniaxial compressive strength, crack initiation stress, crack damage stress and the elastic modulus E of fine-grained sandstone are all significantly higher than the corresponding mechanical parameters of medium-grained sandstone. Therefore, the particle size has an obvious influence on its uniaxial compressive mechanical parameters.

The crack initiation stress and crack damage stress of sandstone obtained in this study are significantly lower than other results in the literatures. The main reason is that the surface of the sampled area has a relatively thick weathered zone. The sandstone blocks in this study were taken from the weathering zone.

4 Comparison of Uniaxial Compression Creep Characteristics of Sandstones with Two Kinds of Particle Size

4.1 Comparison of Creep Deformation Characteristics

The constant loading was adopted in this study, i.e. the axial stress was directly loaded to a predetermined value, and the axial stress was kept unchanged. For medium- and fine-grained sandstone specimens, the applied axial stress was 80%–95% of their corresponding instantaneous uniaxial compressive strengths.

The axial strain and lateral strain changing with time of specimens M6# and L24# are shown in Figs. 4 and 5.

Table 1 Uniaxial compression mechanical parameters of medium-grained sandstone specimens

| No | σ_{ci} (MPa) | σ_{cd} (MPa) | σ_c (MPa) | E (GPa) | μ | σ_{ci}/σ_{ucs} (%) | σ_{cd}/σ_{ucs} (%) |
|---------------|---------------------|---------------------|------------------|-----------|-------|--------------------------------|--------------------------------|
| L1# | 10.6 | 19.3 | 33.4 | 3.98 | 0.20 | 31.7 | 58.4 |
| L2# | 9.3 | 17.9 | 33.0 | 4.14 | 0.22 | 28.2 | 54.2 |
| L3# | 8.8 | 15.1 | 30.0 | 4.13 | 0.23 | 29.3 | 50.3 |
| L4# | 9.1 | 16.8 | 29.6 | 3.96 | 0.19 | 30.6 | 56.7 |
| Average value | 9.5 | 17.3 | 31.5 | 4.05 | 0.21 | 30.0 | 54.9 |

Table 2 Uniaxial compression mechanics parameters of fine-grained sandstone specimens

| No | σ_{ci} (MPa) | σ_{cd} (MPa) | σ_c (MPa) | E (GPa) | μ | σ_{ci}/σ_{ucs} (%) | σ_{cd}/σ_{ucs} (%) |
|---------------|---------------------|---------------------|------------------|-----------|-------|--------------------------------|--------------------------------|
| M1# | 20.3 | 41.8 | 65.0 | 9.8 | 0.16 | 31.2 | 64.3 |
| M2# | 20.8 | 46.4 | 69.9 | 10.5 | 0.14 | 29.7 | 66.4 |
| M3# | 20.7 | 46.4 | 68.2 | 10.3 | 0.15 | 30.3 | 68.1 |
| M4# | 18.7 | 42.2 | 67.4 | 9.7 | 0.13 | 27.8 | 62.6 |
| Average value | 20.1 | 44.2 | 67.6 | 10.1 | 0.15 | 29.8 | 65.4 |

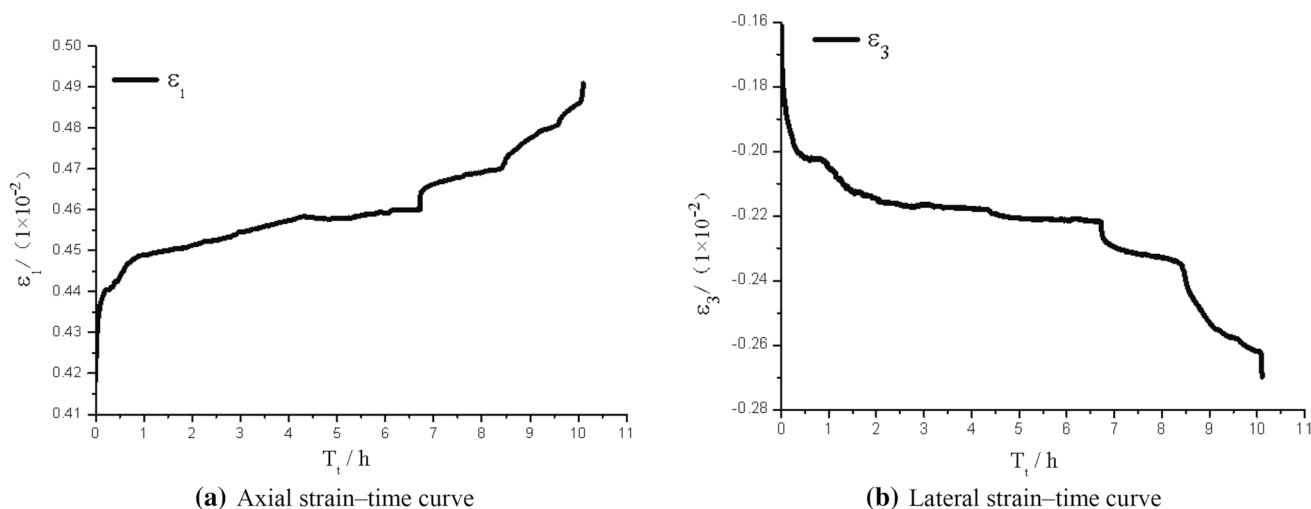


Fig. 4 Axial strain and lateral strain–time curves of fine-grained sandstone specimen M6#

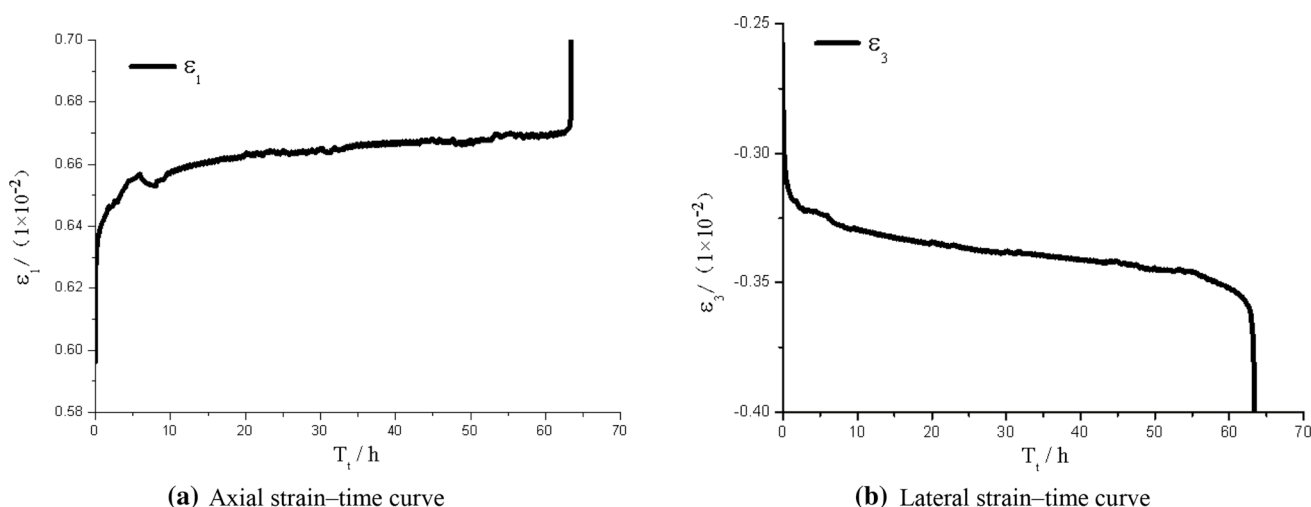


Fig. 5 Axial strain and lateral strain–time curves of medium-grained sandstone specimen L24#

In the figures of this manuscript, the time of the creep test is defined as T_t ; the axial strain of the specimen is defined as ε_1 .

The axial stress applied on medium-grained sandstone specimen L24# is 25.8 MPa, the specimen was destroyed after 63.3 h in the creep stage. The axial stress applied on fine-grained sandstone specimen M6# is 62.8 MPa, and the specimen was destroyed after 10.1 h in the creep stage.

The total axial strain of medium-grained sandstone specimen L24# is $6981 \mu\varepsilon$, the axial instantaneous strain is $5963 \mu\varepsilon$ and the axial creep strain is $1018 \mu\varepsilon$. The axial instantaneous strain and axial creep strain are about 85.4% and 14.6% of the total axial strain, respectively. The total lateral strain of medium-grained sandstone specimen L24# was $4797 \mu\varepsilon$, the lateral instantaneous strain is $2580 \mu\varepsilon$ and the lateral

creep strain is $2217 \mu\varepsilon$. Meanwhile, the lateral instantaneous strain and lateral creep strain account for 53.8% and 46.2% of the total lateral strain, respectively.

The total axial strain of M6# fine-grained sandstone specimen is $4910 \mu\varepsilon$, the axial instantaneous strain is $4182 \mu\varepsilon$ and the axial creep strain is $728 \mu\varepsilon$. The axial instantaneous strain and axial creep strain account for about 85.2% and 14.8% of the total axial strain, respectively. The total lateral strain of L24# medium-grained sandstone specimen is $2699 \mu\varepsilon$, the lateral instantaneous strain is $1610 \mu\varepsilon$ and the lateral creep strain is $1089 \mu\varepsilon$. Meanwhile, the lateral instantaneous strain and lateral creep strain account for 59.7% and 40.3% of the total lateral strain, respectively.

Therefore, the creep deformation of both medium- or fine-grained sandstone specimens in total lateral deformation is

Table 3 Axial, lateral and volumetric creep strains of specimen M6#

| Strain | T_i (h) | ϵ_i ($\mu\epsilon$) | T_s (h) | ϵ_s ($\mu\epsilon$) | T_a (h) | ϵ_a ($\mu\epsilon$) | $\dot{\epsilon}$ (10^{-6} h^{-1}) | ϵ_t ($\mu\epsilon$) | T_t (h) |
|--------------|-----------|--------------------------------|-----------|--------------------------------|-----------|--------------------------------|---|--------------------------------|-----------|
| ϵ_1 | 0.92 | 305 | 7.50 | 207 | 1.69 | 216 | 27.6 | 728 | 10.11 |
| ϵ_3 | 1.58 | 517 | 6.84 | 225 | 1.69 | 347 | 32.9 | 1089 | 10.11 |
| ϵ_v | 2.00 | 743 | 6.42 | 221 | 1.69 | 486 | 34.4 | 1450 | 10.11 |

Table 4 Axial, lateral and volumetric creep strains of specimen L24#

| Strain | T_i (h) | ϵ_i ($\mu\epsilon$) | T_s (h) | ϵ_s ($\mu\epsilon$) | T_a (h) | ϵ_a ($\mu\epsilon$) | $\dot{\epsilon}$ (10^{-6} h^{-1}) | ϵ_t ($\mu\epsilon$) | T_t (h) |
|--------------|-----------|--------------------------------|-----------|--------------------------------|-----------|--------------------------------|---|--------------------------------|-----------|
| ϵ_1 | 11.2 | 624 | 50.05 | 112 | 2.08 | 305 | 2.2 | 1018 | 63.33 |
| ϵ_3 | 9.8 | 715 | 45.5 | 166 | 8.13 | 1336 | 3.7 | 2217 | 63.33 |
| ϵ_v | 10.1 | 810 | 43.1 | 197 | 10.13 | 2409 | 4.6 | 3416 | 63.33 |

Table 5 Relationship between the mechanical parameters and creep failure time of medium-grained sandstone specimens

| No | σ_{cp} (MPa) | $\bar{\sigma}_c$ (MPa) | $\sigma_{cp}/\bar{\sigma}_c$ (%) | T_t (min) | $\bar{\sigma}_{cd}$ (MPa) | $\bar{\beta}$ |
|------|---------------------|------------------------|----------------------------------|-------------|---------------------------|---------------|
| L5# | 27.8 | 31.5 | 88.3 | 1004.7 | 17.3 | 1.607 |
| L7# | 28.0 | 31.5 | 88.9 | 106.2 | 17.3 | 1.618 |
| L24# | 25.8 | 31.5 | 81.9 | 3799.8 | 17.3 | 1.491 |

Table 6 Relationship between the mechanical parameters and creep failure time of fine-grained sandstone specimens

| No | σ_{cp} (MPa) | $\bar{\sigma}_c$ (MPa) | $\sigma_{cp}/\bar{\sigma}_c$ (%) | T_t (min) | $\bar{\sigma}_{cd}$ (MPa) | $\bar{\beta}$ |
|------|---------------------|------------------------|----------------------------------|-------------|---------------------------|---------------|
| M5# | 57.5 | 67.6 | 85.1 | 45.4 | 44.2 | 1.301 |
| M6# | 62.8 | 67.6 | 92.9 | 606.3 | 44.2 | 1.421 |
| M16# | 60.8 | 67.6 | 89.9 | 29.5 | 44.2 | 1.376 |

more obvious than the creep deformation in total axial deformation. On the other hand, during the creep process, the creep deformation of the medium-grained sandstone specimen is higher than that of the fine-grained sandstone specimen, indicating that creep deformation less likely occurs in the sandstone with smaller and more average particle size.

We define T_i , T_s , T_a and T_t as the transient creep time, steady-state creep time, accelerated creep time and total creep time. Meanwhile, ϵ_i , ϵ_s and ϵ_a represent the creep strain of the specimen during the transient, steady-state and accelerated creep stages, respectively. In addition, ϵ_t represents the total creep strain of the specimen during the creep stage and $\dot{\epsilon}$ represents the steady-state creep rate of the specimens.

The axial, lateral and volumetric creep strains of fine-grained sandstone specimen M6# are shown in Table 3. The axial, lateral and volumetric creep strains of medium-grained sandstone specimen L24# are shown in Table 4.

The axial creep strain during the transient creep stage is the highest, followed by the accelerated creep stage, the axial creep strain during the steady-state creep stage is the lowest. The lateral creep strain during the accelerated creep stage is the highest, followed by the transient creep stage, and then the steady-state creep stage. The volumetric creep strain during the accelerated creep stage is the highest, followed by the

transient creep stage, and the volumetric creep strain during the steady-state creep stage is the lowest. The rank of each creep strain during different stages is the same in medium and fine-grained sandstone specimens.

Therefore, the damage of both medium-grained and fine-grained sandstone specimens during the creep process mainly occurs in the transient creep stage and the accelerated creep stage.

4.2 Comparison of Creep Failure Time

We define $\bar{\beta}$ as the ratio of the applied creep stress to the average value of the crack damage stress during the creep test (Tables 1 and 2), the crack damage stresses of medium- and fine-grained sandstone specimens are 17.3 MPa and 44.2 MPa, respectively. The relationship between the mechanical parameters and creep failure time of the medium-grained and fine-grained sandstone specimens obtained through the experiments is shown in Tables 5 and 6.

In Tables 5 and 6, σ_{cp} is creep stress; $\bar{\sigma}_c$ is average uniaxial compressive strength; $\bar{\sigma}_{cd}$ is average critical damage stress.

For both the medium- and fine-grained sandstone specimens, the creep failure time decreases with increasing $\bar{\beta}$.

5 Comparison of AE Characteristics During the Compression Creep Process of Sandstones

5.1 Acoustic Emission Amplitude

The relationships between the AE amplitude and axial strain of specimens M6# and L24# are shown in Fig. 6.

During the transient creep stage, the AE amplitude of the fine-grained sandstone specimen decreases with increasing time and then became steady (Fig. 6). The value of AE amplitude at this stage keeps at a higher level, indicating that internal microcracks and weak structural planes inside the fine-grained sandstone specimen initiate and expand. However, the initiation and propagation of microcracks decrease with time, and the axial strain curves also appear to be stable with time. In the steady-state creep stage, the AE amplitude of fine-grained specimens is in a “uniform” distribution within a certain range, and the value of the AE amplitude remained at a low level. This indicates that new microcracks and weak structural planes inside the specimens are decreasing, and the creep rate tends to be stable. After processing to the accelerated creep stage, there was a significant “sudden rise” in the amplitude of the acoustic emissions at the boundary between steady state and accelerated creep stage. The AE amplitude increases significantly at this boundary. It then drops quickly and grows slowly after entering the accelerated creep stage. The value and activity of the AE amplitude of the specimens in the accelerated creep stage are significantly higher than those values in the transient and steady-state creep stages. When the specimen is broken, the value of the AE amplitude rises to the maximum for the entire creep stage. This indicated that a large number of cracks are generated inside the specimen at this stage and

merge into the main fracture surface until the specimen is destroyed.

The AE amplitude characteristics of medium-grained sandstone specimen are similar to those of fine-grained sandstone, and the creep deformation of medium-grained sandstone specimen is greater than that of fine-grained sandstone specimen.

The AE amplitude of both fine-grained and medium-grained sandstone specimens in the accelerated creep stage is higher than it in the transient and steady-state creep stages. The AE amplitude directly relates to the creep rate of sandstone specimen.

5.2 AE Ring-Down Count Rate

The relationship between the AE ring-down count rate and axial strain of specimens M6# and L24# is shown in Fig. 7.

During the creep process, the AE amplitude and AE ring-down count rate of fine- and medium-grained sandstone specimen have similar variations: (1) in the transient creep stage, the AE ring-down count rate of the specimen decreases with time and then become stable; (2) in the steady-state creep stage, the AE ring-down count rate of specimen is maintained at a relatively low level; (3) at the transition point between the steady-state and accelerated creep stages, the AE ring-down count rate increases significantly and then decreases with increasing time; (4) after entering the accelerated creep phase, the AE ring-down count rate of the specimen is significantly greater than that in the transient and steady-state creep stages; (5) the AE ring-down count rate reaches its maximum for the entire creep stage when damage occurs in the specimen. This conclusion is consistent with Zhao et al. [10].

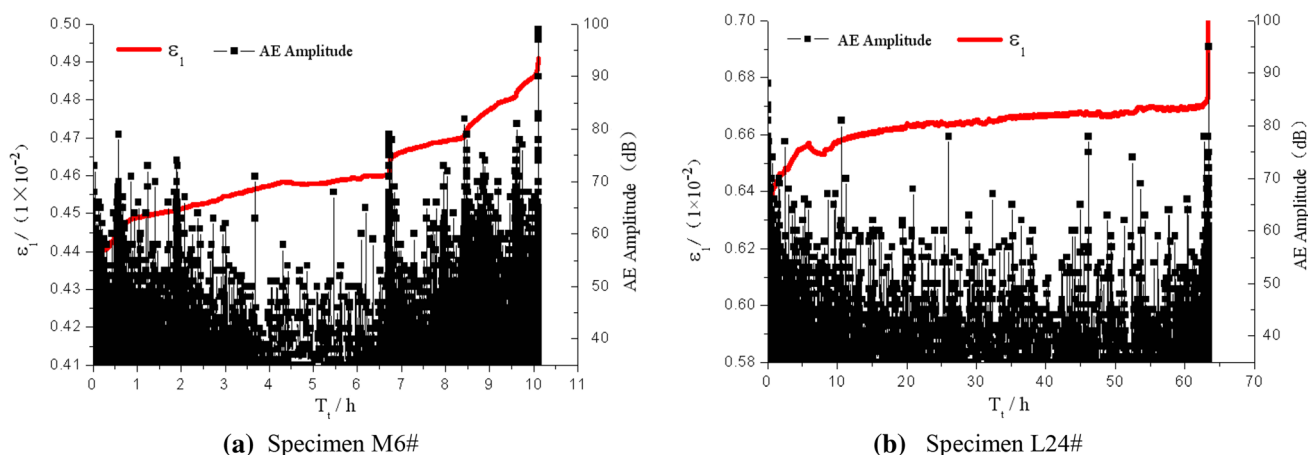


Fig. 6 Relationship between the AE amplitude and axial strain of specimens M6# and L24#

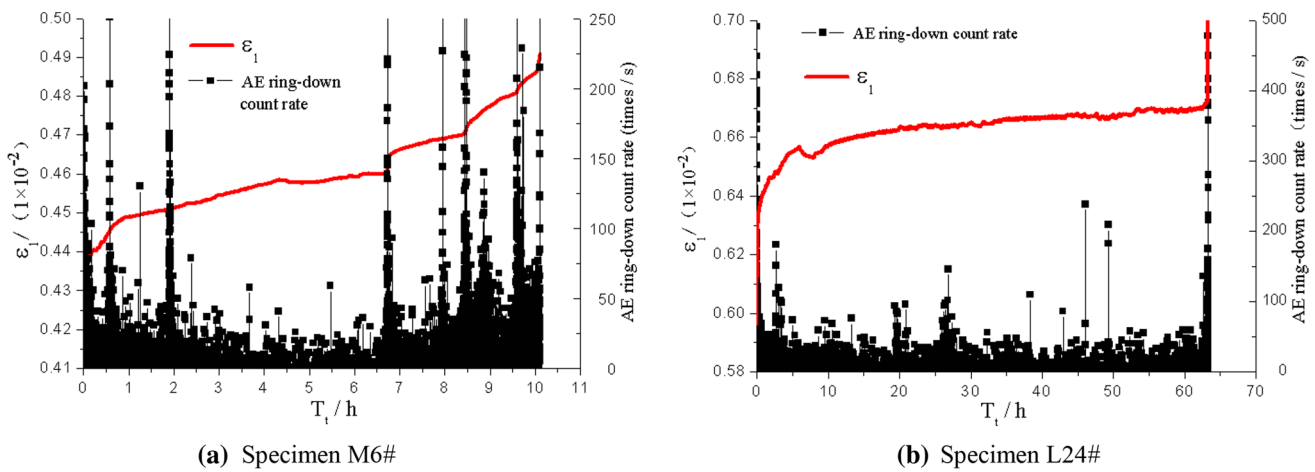


Fig. 7 Relationship between the AE ring-down count rate and axial strain of specimens M6# and L24#

5.3 Acoustic Emission Event Rate

The AE event rate refers to the sum of AE events generated within a certain period of time, which is closely related to the activity frequency of microcracks inside the rock material.

The relationship between the AE event rate and axial strain of specimens M6# and L24# is shown in Fig. 8.

During the creep process, the AE event rates of both fine- and medium-grained sandstone specimens have a similar variation law with the AE ring-down count rate.

5.4 Value of $\sum N/\sum E$ of Acoustic Emissions

The parameter $\sum N/\sum E$ was used in this study to further analyse micro-crack evolution. This parameter represents the ratio of the accumulative hits ($\sum N$) and the cumulative

energy ($\sum E$) [21–23]. The energy contained in the AE signal is inversely proportional to the value of this parameter. That is, the greater the energy contained in each AE signal, the smaller the $\sum N/\sum E$ ratio. Wang et al. [21] found that the mutation point in the $\sum N/\sum E$ curve could be taken as an indicator of the crack damage threshold of Granite. Hall et al. [22] found that the increasing $\sum N/\sum E$ indicates that a large number of low-energy, high-frequency cracks are generated inside the rock specimen, but the evolution of these micro-cracks does not directly affect the final damage of the rock. The decreasing of $\sum N/\sum E$ indicates a small amount of AE high-energy events are generated inside the rock specimen, which is the initiation or connection of large-scale cracks that may constitute direct damage to the rock. Therefore, the parameter $\sum N/\sum E$ can be used to evaluate the evolution of microcracks in rock materials during the loading process.

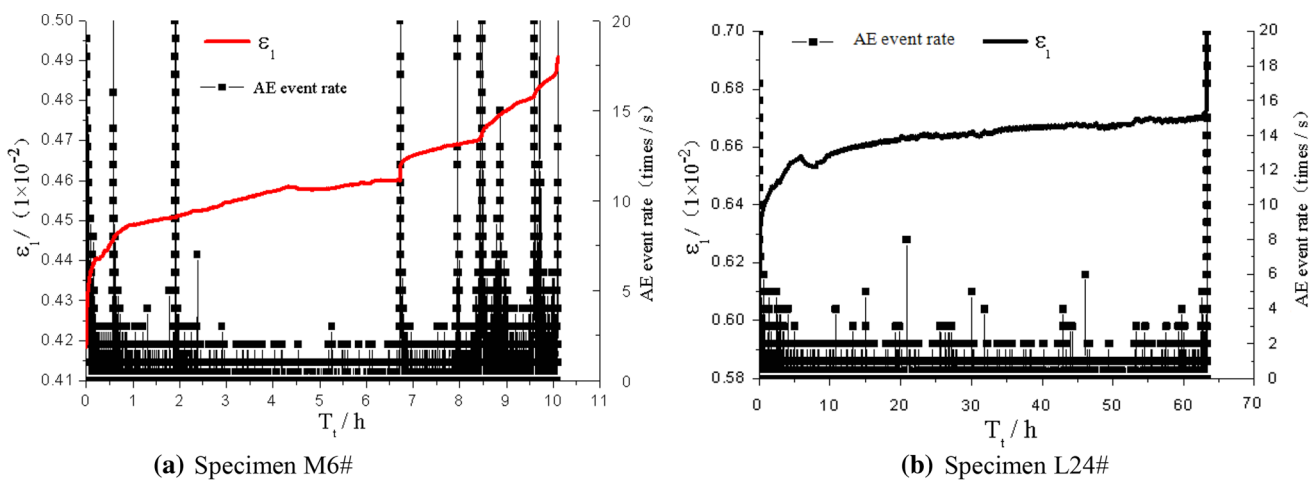


Fig. 8 Relationship between the AE event rate and axial strain of specimens M6# and L24#

In this study, $\sum N/\sum E$ ratio is defined as the AE-*r* value [23]. The relationship between the AE-*r* value and axial strain of fine-grained sandstone specimens M5#, M6# and

M16# is shown in Fig. 9, and the relationship between the AE-*r* value and axial strain of medium-grained sandstone specimens L5# and L24# is shown in Fig. 10.

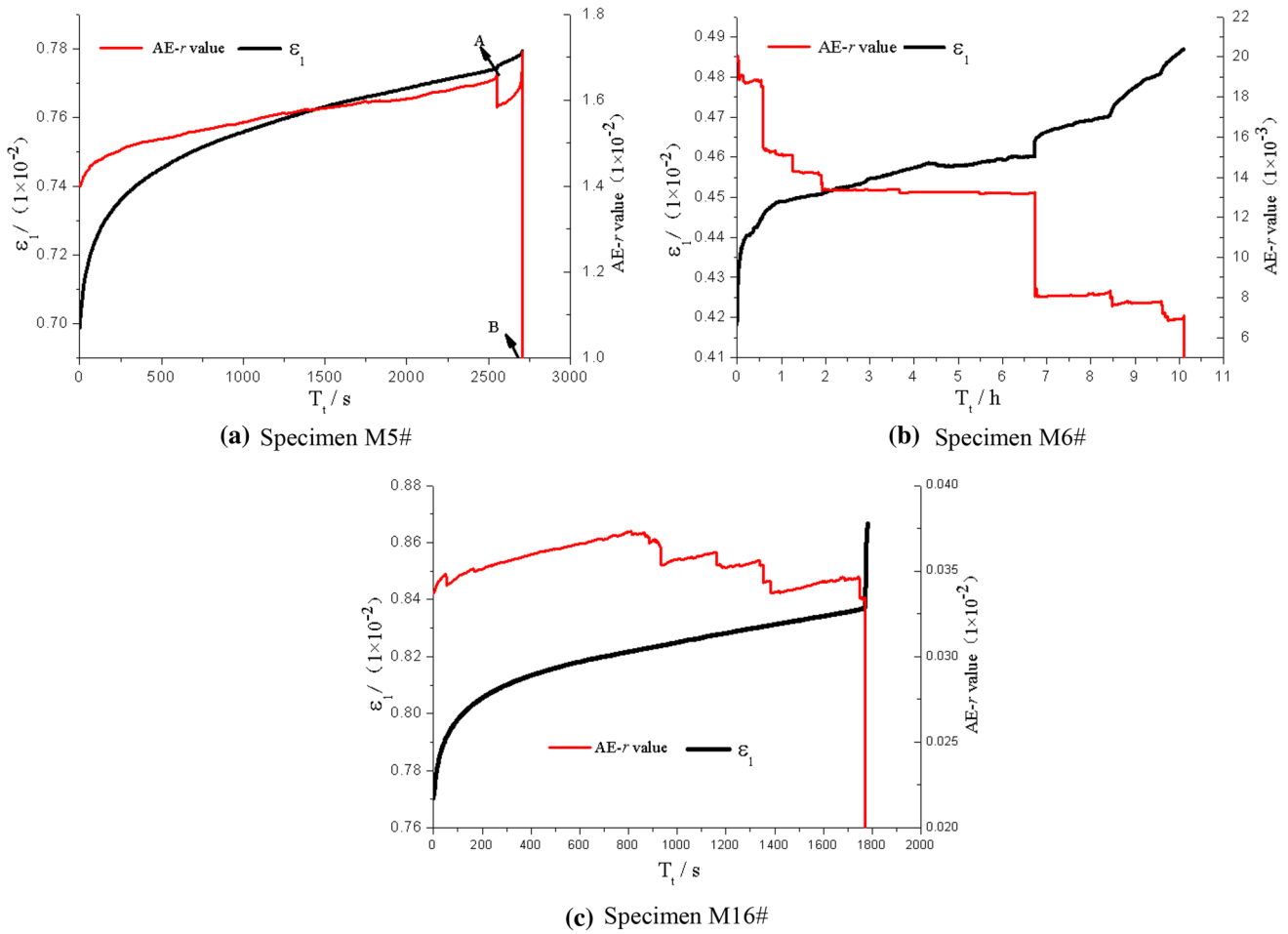


Fig. 9 Relationship between the AE-*r* value and axial strain of fine-grained sandstone specimens

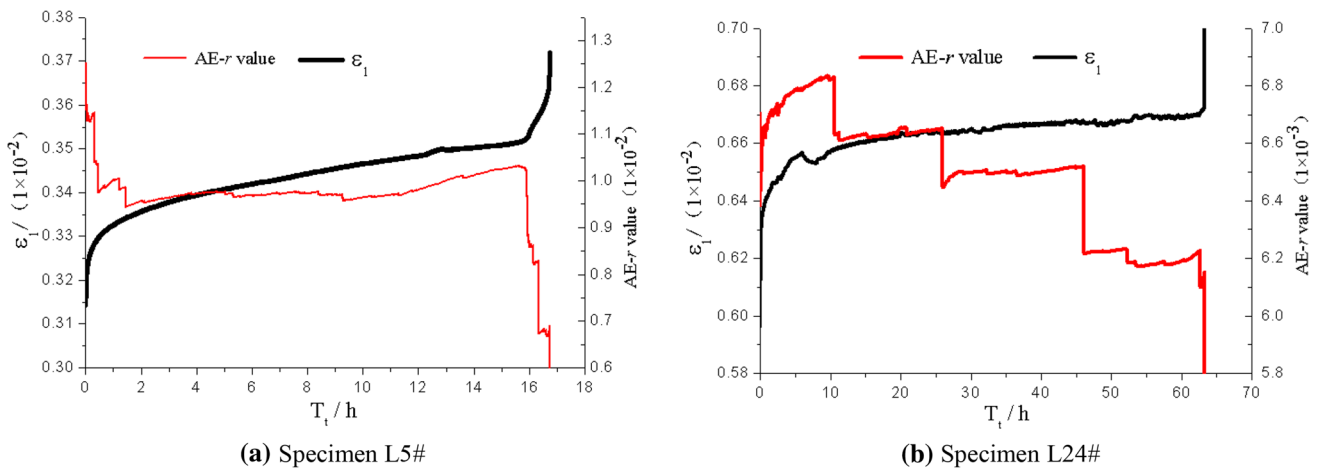


Fig. 10 Relationship between the AE-*r* value and axial strain of medium-grained sandstone specimens

The AE- r values of fine- and medium-grained sandstone specimens have no obvious variation trend with axial strain in the transient and steady-state creep stages. However, they keep at a high level in the steady-state creep stage, and the AE- r value is also relatively stable and lower than that in transient creep stage. Therefore, in the transient creep stage, the internal microcracks of fine- and medium-grained sandstone specimens are mainly dominated by small-scale crack initiation and propagation, where the microcracks are densely active. In the steady-state creep stage, the activity frequency of internal microcracks is decreasing, dominated by large-scale microcrack initiation and propagation, and the initiation and propagation speed of microcracks is relatively stable.

When fine- and medium-grained sandstone specimens enter the accelerated creep stage from the steady-state creep stage, there is an obvious “sudden drop” in the AE- r value. And the AE- r value falls to the lowest point when the specimen is destroyed. Therefore, the experiment result shows that the microcracks are mainly dominated by large-scale microcrack initiation and propagation in the accelerated creep stage.

We define point A as the boundary between the steady-state and accelerated creep stages, B as the point at the lowest r value during the creep process. The AE- r values corresponding to point A of fine-grained sandstone specimens M5#, M6# and M16# are 1.67×10^2 , 8.1×10^3 and 3.3×10^2 , respectively. The AE- r values corresponding to point A of medium-grained sandstone specimens L5# and L24# are 1.03×10^2 and 6.25×10^3 , respectively. The AE- r values at point A of two kinds of sandstone specimens are close to each other, indicating that their microcrack activity scales are quite similar when entering the accelerated creep stage.

The AE- r values corresponding to point B of fine-grained sandstone specimens M5#, M6# and M16# were 1.35×10^4 , 2.43×10^4 and 4.5×10^4 , respectively. The AE- r values corresponding to point B of medium-grained sandstone specimens L5# and L24# are 3.46×10^3 and 5.07×10^3 , respectively. The difference between the AE- r values of two kinds of sandstone at the end of the accelerated creep stage is about one order of magnitude; it indicates that microcracks in fine-grained sandstone specimen have a higher activity scale than those of medium-grained sandstone specimen in the accelerated creep stage.

6 Conclusions

- (1) The microstructure of fine-grained sandstone is the granular sand-like structure, and the medium-grained sandstone has a grain-like microstructure.
- (2) The mechanical parameters such as uniaxial compressive strength, crack initiation stress, crack damage

stress and elastic modulus E of fine-grained sandstone specimen are all significantly higher than the corresponding mechanical parameters of medium-grained sandstone specimen.

- (3) The creep deformation of the medium-grained sandstone specimen is higher than that of the fine-grained sandstone specimen, indicating that the sandstone with smaller and the more well sorted particle size is less likely to produce creep deformation.
- (4) The damage to both medium- and fine-grained sandstone specimens during the creep process mainly occurs in the transient and accelerated creep stages.
- (5) The AE amplitude, AE event rate and AE ring-down count rate of both the medium- and fine-grained sandstone specimens have similar change laws during creep stages.
- (6) The AE- r value of these two kinds of sandstone specimens during the transient creep stage is generally higher than that in the steady-state creep stage, and the AE- r value is relatively stable in the steady-state creep stage. When these two kinds of sandstone specimens enter the accelerated creep stage from the steady-state creep stage, there is an obvious “sudden drop” in the AE- r value; it falls to the lowest point when the specimens are destroyed.

Acknowledgements This work was supported by the National Natural Science Foundation of China (Grant Nos. 51664018, 41002108), and the Systematic Project of Guangxi Key Laboratory of Disaster Prevention and Engineering Safety (Grant No. 2019ZDK051).

References

1. Xiong, L.X.; Li, T.B.; Yang, L.D.: Biaxial compression creep test on greenschist considering the effects of water content and anisotropy. *KSCE J. Civil Eng.* **18**(1), 103–112 (2014)
2. Chen, J.W.: Creep mechanical behavior of silty mudstone under complicated geological conditions. *J. Yangtze River Sci. Res. Inst.* **35**, 102–107 (2018)
3. Ohnaka, M.: Acoustic emission during creep of brittle rock. *Int. J. Rock Mech. Mining Sci.* **20**, 121–134 (1983)
4. Yang, Y.J.; Wang, D.C.; Zhao, N.N.; Chen, S.J.: Acoustic emission characteristics of coal creep under step load. *J. Basic Sci. Eng.* **21**, 159–166 (2013)
5. Gong, C.; Li, C.H.; Zhao, K.: Acoustic emission characteristics during short-time creep process of red sandstone under different stress level. *J. Northeast. Univ. (Nat. Sci.)* **36**, 1347–1352 (2015)
6. Chen, C.F.; Xu, T.; Heap, M.J.; Baud, P.: Influence of unloading and loading stress cycles on the creep behavior of Darley Dale sandstone. *Int. J. Rock Mech. Mining Sci.* **112**, 55–63 (2018)
7. Li, P.: Experimental study on creep damage of sandstone based on acoustic emission tests. *J. Yangtze River Sci. Res. Inst.* **35**, 78–83 (2018)
8. Shi, G.C.; Yang, X.J.; Yu, H.C.; Zhu, C.: Acoustic emission characteristics of creep fracture evolution in double-fracture fine



- sandstone under uniaxial compression. *Eng. Fract. Mech.* **210**, 13–28 (2019)
9. Zhu, W.C.; Li, S.H.; Li, S.; Niu, L.L.: Influence of dynamic disturbance on the creep of sandstone: an experimental study. *Rock Mech. Rock Eng.* **52**, 1023–1039 (2019)
 10. Zeng, Y.; Liu, J.F.; Zhou, Z.W.; Wu, C.; Li, Z.C.: Study on creep acoustic emission and damage evolution of salt rock under uniaxial compression. *Rock Soil Mech.* **40**, 207–215 (2019)
 11. Paraskevopoulou, C.; Perras, M.; Diederichs, M.; Loew, S.; Lam, T.; Jensen, M.: Time-dependent behaviour of brittle rocks based on static load laboratory tests. *Geotech. Geol. Eng.* **36**, 337–376 (2018)
 12. Nicksiar, M.; Martin, C.D.: Crack initiation stress in low porosity crystalline and sedimentary rocks. *Eng. Geol.* **154**, 64–76 (2013)
 13. Xue, L.; Qin, S.Q.; Sun, Q.; Wang, Y.Y.; Lee, L.M.; Li, W.C.: A study on crack damage stress thresholds of different rock types based on uniaxial compression tests. *Rock Mech. Rock Eng.* **47**, 1183–1195 (2015)
 14. Kim, J.S.; Lee, K.S.; Cho, W.J.; Choi, H.J.; Cho, G.C.: A comparative evaluation of stress-strain and acoustic emission methods for quantitative damage assessments of brittle rock. *Rock Mech. Rock Eng.* **48**, 495–508 (2015)
 15. Pepe, G.; Mineo, S.; Pappalardo, G.; Cevasco, A.: Relation between crack initiation-damage stress thresholds and failure strength of intact rock. *Bull. Eng. Geol. Environ.* **77**, 709–724 (2018)
 16. Li, X.F.; Li, H.B.; Liu, L.W.; Liu, Y.Q.; Ju, M.H.; Zhao, J.: Investigating the crack initiation and propagation mechanism in brittle rocks using grain-based finite-discrete element method. *Int. J. Rock Mech. Mining Sci.* **127**, 104219 (2020)
 17. Zhang, G.K.; Li, H.B.; Wang, M.Y.; Li, X.F.: Crack initiation of granite under uniaxial compression tests: a comparison study. *J. Rock Mech. Geotech. Eng.* **127**, 656–666 (2020)
 18. Eberhardt, E.; Stead, D.; Stimpson, B.; Read, R.S.: Identifying crack initiation and propagation thresholds in brittle rock. *Can. Geotech. J.* **35**, 222–233 (1998)
 19. Chen, G.Q.; Wang, J.C.; Li, J.; Li, T.B.; Zhang, H.: Influence of temperature on crack initiation and propagation in granite. *Int. J. Geomech.* **18**, 04018094(1)-04018094(14) (2018)
 20. Zhu, J.; Deng, J.H.; Huang, Y.M.; He, Z.L.: Influence of water on the fracture process of marble with acoustic emission monitoring. *KSCE J. Civil Eng.* **23**, 3239–3249 (2019)
 21. Wang, Z.L.; He, A.L.; Shi, G.Y.; Mei, G.X.: Temperature effect on AE energy characteristics and damage mechanical behaviours of granite. *Int. J. Geomech.* **18**(3), 04017163(1)-04017163(10) (2018)
 22. Hall, S.A.; Sanctis, F.D.; Viggiani, G.: Monitoring fracture propagation in a soft rock (Neapolitan Tuff) using acoustic emissions and digital images. *Pure Appl. Geophys.* **163**, 2171–2204 (2006)
 23. Zhao, K.; Zhu, Z.C.; Zeng, P.; Chen, S.J.: Experimental study on acoustic emission characteristics of phyllite specimens under uniaxial compression. *J. Eng. Sci. Technol. Rev.* **8**(3), 53–60 (2015)

